Numerical study of the thermal ablation of wet solids by ultrashort laser pulses

Danny Perez,[1,*] Laurent Karim Béland,[1] Delphine Deryng,[1] Laurent J. Lewis,[1,†] and Michel Meunier[2,‡]
[1]*Département de Physique et Regroupement Québécois sur les Matériaux de Pointe (RQMP), Université de Montréal, Case Postal 6128, Succursale Centre-Ville, Montréal, Québec, Canada H3C 3J7*
[2]*Laboratoire de Procédés par Laser, Département de Génie Physique et Regroupement Québécois sur les Matériaux de Pointe (RQMP), École Polytechnique de Montréal, Case Postal 6079, Succursale Centre-Ville, Montréal, Québec, Canada H3C 3A7*
(Received 1 June 2007; revised manuscript received 26 October 2007; published 24 January 2008)

The ablation by ultrashort laser pulses at relatively low fluences (i.e., in the thermal regime) of solids wetted by a thin liquid film is studied using a generic numerical model. In comparison with dry targets, the liquid is found to significantly affect ablation by confining the solid and slowing down the expansion of the laser-heated material. These factors affect the relative efficiency of the various ablation mechanisms, leading, in particular, to the complete inhibition of phase explosion at lower fluences, a reduced ablation yield, and significant changes in the composition of the plume. As a consequence, at fluences above the ablation threshold, the size of the ejected nanoclusters is lower in presence of the liquid. Our results provide a qualitative understanding of the effect of wetting layers on the ablation process.

DOI: 10.1103/PhysRevB.77.014108 PACS number(s): 61.80.Az, 78.20.Bh

I. INTRODUCTION

Laser ablation—the collective ejection of material from a target following irradiation by short, intense bursts of light—is a technology widely used in many applications such as thin film deposition and cleaning, surface micromachining, laser surgery, mass spectrometry, etc.[1] It is also an efficient method for the controlled production of nanoparticles. In this respect, one can distinguish between the direct ablation of a solid target in vacuum (or in a gaseous environment), where the target can expand freely, and "confined" ablation, where the target is immersed in a liquid such as water. In the latter case, depending on the nature of the target and the liquid, clusters of various sizes are more or less dispersed in the liquid, forming a colloidal solution which could have potential biomedical applications (see Refs. 2 and 3 for a general overview of the subject). Ultrafast lasers have recently been used to produce colloidal suspensions of very fine (a few nanometers) gold nanoparticles in pure water, which are very difficult to fabricate by other methods.[4–6] While it has been shown experimentally that the chemical nature and the thickness of the immersing liquid influence the morphology, composition, and size distribution of the clusters, these effects are not well understood.[2]

The physics of ablation in vacuum has been studied in detail both experimentally[7–9] and theoretically;[10–20] recent numerical models by Perez and co-workers[14,16–18] and Lorazo *et al.*,[15,19,20] in particular, have provided a comprehensive picture of the mechanisms underlying ablation in the thermal regime. It has been demonstrated that ablation can occur through different processes, viz., spallation, phase explosion (whereby a thermodynamically metastable homogeneous liquid decomposes into a mixture of liquid droplets and gas), fragmentation (disintegration of a homogeneous material into clusters under the action of large strain rates), or vaporization, as a function of increasing fluence.[16] Also, it has been shown that, in the case of very long (nanosecond) pulses in molecular solids, the route to ablation is largely determined by the degree of local confinement, i.e., depth into the target;[18] this turns out to be of utmost relevance to the present study. In contrast, the corresponding problem in presence of a liquid layer remains largely unexplored: there exists, to our knowledge, only a few numerical studies of "wet" targets at subthreshold fluences (i.e., below the threshold for ablation);[21,22] these evidently do not cover the ablation regime which is of importance for understanding the formation of clusters.

In order to assess the effect of the presence of a liquid film on the ablation process, we report in this paper the results of a numerical study of ultrafast femtosecond laser ablation in a solid covered by a thin liquid layer, and compare the results with the case of a dry target. We limit the study to relatively low fluences where the thermal regime is predominant and ignore any role of the resulting plasma which would become important at higher fluences. Anticipating our results, we find that the main effect of the liquid is to confine the solid target over long time scales and to subsequently slow down its expansion. This severely restricts the efficiency of some of the ablation mechanisms, in particular, phase explosion. Changes in the relative importance of the different mechanisms in turn reduce the ablation yield, strongly affecting the properties of the plume. We also show that the dynamics of the liquid film is largely dominated by the propagation of the pressure waves emitted at the interface with the solid target.

II. COMPUTATIONAL DETAILS

For the present study we employ the model proposed by Perez and Lewis,[14,16] which was successfully used to investigate ablation in a variety of situations and, in particular, to unveil a new mechanism for ablation, viz., fragmentation. This model is based on a two-dimensional system of Lennard-Jones atoms whose evolution in time is followed using molecular-dynamics (MD) simulations. The laser pulse, Gaussian in time and of duration Δt, is modeled as a sequence of discrete photons absorbed by the target according to the Beer-Lambert law, $I(z)=I_0e^{-z\alpha}$, where the depth z

is measured from the surface of the solid—we will assume the liquid to be transparent—and α is the absorption coefficient. The energy of the photons is transferred to carriers which obey a Drude-like dynamics, eventually giving up their energy to atoms via carrier-phonon interactions. Note that the passage of a pulse can induce optical breakdown in the liquid, thus making it able to absorb part of the laser light; when this occurs, thermoelastic pressure waves can be emitted from the fluid, potentially affecting the ablation dynamics. These effects are not considered here since we are focusing on the thermal regime where they are expected to be small.

As mentioned above, the atoms interact via the Lennard-Jones potential, $\phi_{LJ}(r)=4\epsilon[(\sigma/r)^{12}-(\sigma/r)^{6}]$, appropriately corrected to vanish at the cutoff distance $r_c=2.5\sigma$. The parameters σ (characteristic length) and ϵ (characteristic energy) are chosen so as to represent either a solid or a liquid, as well as cross interactions between the two. In practice, two different cases were considered, namely, a high-density liquid with $\sigma'_{\ell\ell}=\sigma_{ss}$ and a low-density liquid with $\sigma''_{\ell\ell}=3\sigma_{ss}$; in both situations we set $\epsilon_{\ell\ell}=\epsilon_{ss}/10$. For the cross terms we set $\sigma'_{s\ell}=\sigma'_{\ell\ell}$, $\sigma''_{s\ell}=\sigma''_{\ell\ell}$, and $\epsilon_{s\ell}=\epsilon_{\ell\ell}$. The atoms are assumed to all have the same mass. Evidently, with this choice of parameters, the densities of the solid and the liquid are the same in the first case, and differ by a factor of 9 in the second case. The high-density liquid is thus, "densitywise," akin to the molten phase of the target material, and the low-density to a typical solvent. This choice allows us to consider the effect of varying the compressibility of the liquid, thus providing different levels of confinement for the solid material. Of course, one could instead have opted for different masses for the liquid and solid atoms in order to vary the inertial confinement; a thorough study of the behavior of the system in the multidimensional parameter space is, however, beyond the scope of the present work.

Previous studies have clearly established that the relevant physics in the thermal regime—which is that we are concerned with here—is determined by general features of the temperature-density phase diagram,[14–16,20] which can be obtained for different Lennard-Jones substances by rescaling the characteristic parameters σ and ϵ; thus, in what follows, the thermodynamic data are presented in reduced units, as is usual for such studies (see, e.g., Ref. 23). The correspondence with real materials can then be obtained by assigning specific values to σ and ϵ. Thus, in practice, two different temperature scales are used here, viz., $T_s^*=\epsilon_{ss}$ for the (solid) target and $T_\ell^*=\epsilon_{\ell\ell}$ for the (liquid) film. Likewise, for the densities, we have $\rho_s^*=(\sigma_{ss})^{-2}$, and $\rho_\ell'^*=(\sigma'_{\ell\ell})^{-2}$ and $\rho_\ell''^*=(\sigma''_{\ell\ell})^{-2}$ for the high- and low-density liquids, respectively. In these units, the critical point is $(0.35\rho^*,0.4549T^*)$, and the triple line is at $T=0.38T^*$ for densities ρ^* between 0.027 and 0.76. For other quantities, the properties of the solid are used as reference, i.e., σ_{ss} for length and position, ϵ_{ss} for energy, and $\tau^*=(m_{ss}/\epsilon_{ss}\sigma_{ss}^2)^{1/2}$ for time (where m is the mass of the atoms). For clarity, the units will be specified whenever necessary.

As noted above, contact with real materials can be made by assigning some specific values to ϵ and σ. For a typical close-packed metal, we would have $\sigma=2-3$ Å and $\epsilon\sim 1$ eV. These parameters are such that solid-liquid coexistence is possible at the initial temperature of the target (roughly room temperature for the above parameters). We have set $\alpha\sim 0.01\sigma^{-1}$ and $\Delta t=\tau^*$, corresponding typically to a penetration depth of a few hundred angstroms and a pulse duration of a few hundred femtoseconds. Concerning the fluence, comparison with "real" values is difficult given the two-dimensional nature of our model; in practice, it is more relevant to compare the fluence with the threshold value for ablation to take place, $F_{\rm th}$.

The models are constructed in a slab geometry, 200 atomic layers in width (x direction) by 400 layers in thickness (z direction) for the solid, and same width and a thickness of $500\sigma_{ss}$ for the liquid, for both densities. Periodic boundary conditions are imposed in the x direction, while absorbing boundary conditions are used at the bottom of the solid to eliminate the reflection of pressure waves generated by the pulses and traveling toward the bulk.[24] All samples are equilibrated properly before light impinges on the surface of the solid (initially at $z=0$).

Before moving on with the results, we emphasize that previous studies[14,16] and comparison with three-dimensional simulations[15] have shown that this two-dimensional model contains the essential physics of ablation, while offering the enormous advantage of much larger systems to be dealt with over longer time scales than more realistic models. Our model should be viewed as generic: while it does not allow a detailed description of real materials, it does provide understanding of the physical processes at the fundamental level. One obvious limitation is that it cannot account for plasma formation; we thus restrict our study to the low-fluence thermal regime, which is below $\sim 5F_{\rm th}$ in "dry" conditions.[7] While ionization can occur at low fluence (particularly in the liquid), we do not expect this to significantly affect the ablation behavior in the thermal regime. Furthermore, temperature-induced changes in the reactivity of the liquid cannot be taken into account by empirical potentials; as such, the effect of etching and of other chemical reactions[25] is not considered here. Our objective being to rationalize the physics underlying ablation in the thermal regime—not to provide a detailed description of the formidably complex processes taking place in real materials—such approximations are warranted. As a final point, the liquid layer here is significantly thinner than in a typical experimental (tens of nanometers vs 1–10 mm); we nevertheless expect our results to give a proper description of the influence of the liquid layer on the ablation mechanism since the conclusions easily extrapolate to larger thicknesses.

III. RESULTS

We will first describe the evolution of the (dense) liquid film following irradiation by the laser and see that this is primarily driven by the passage of strong pressure waves originating from the interface region. Next, we will examine the behavior of the solid target, taking the dry sample as a reference. The main effect of the presence of the liquid layer is to slow down the expansion of the material, leading to smaller ablation yields and the suppression of phase explo-

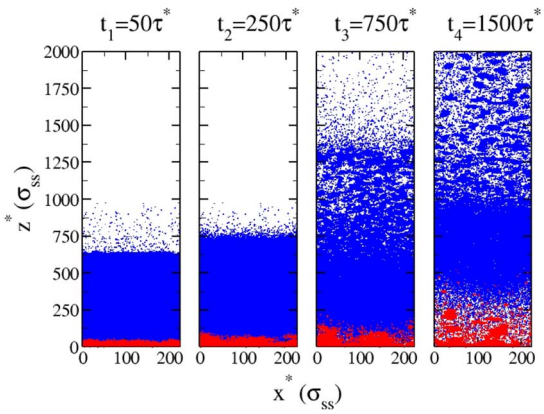

FIG. 1. (Color online) Snapshots of a simulation of the solid target (red dots, bottom) wetted by the high-density liquid (blue dots, top) at a fluence of $560\epsilon_{ss}/\sigma_{ss}$. The surface of the target is initially at $z^*=0$.

sion as a possible ablation mechanism. Finally, the impact of the liquid film on the ablation plume from the point of view of both cluster yield and composition will be examined.

A. Liquid film

The behavior of the high-density liquid wetting a solid target, following irradiation with the laser pulse at a fluence $F=560\epsilon_{ss}/\sigma_{ss}$ (above the ablation threshold, $F_{\text{th}} \sim 300\epsilon_{ss}/\sigma_{ss}$), is illustrated in Figs. 1 and 2. The laser energy is absorbed by the upper layers of the solid—not by the liquid as it is assumed to be transparent. (Multiphoton absorption may occur at relatively low fluence in liquids; however, the resulting increase in temperature is unlikely to affect ablation significantly in the range of fluences considered here.) An analysis of the temperature and pressure in the interface region shows these two quantities to increase rapidly and dramatically in reaction to the large amount of energy injected into the system on a very short time scale. Because the target (solid) material is inertially confined on time scales shorter than a few tens of τ^* (a few picoseconds),

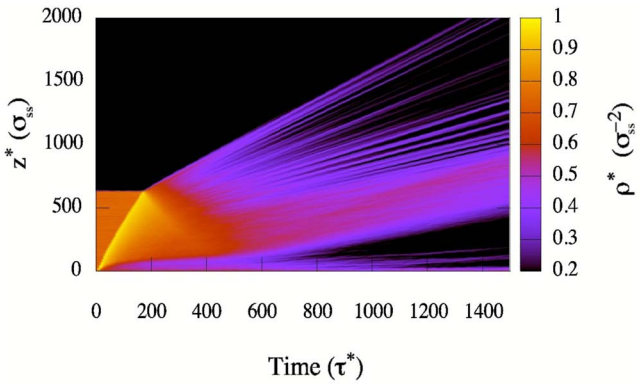

FIG. 2. (Color online) Evolution of the density of the (high-density) liquid film for the simulation presented in Fig. 1 (cf. color scale on the right).

as also is the case for dry targets, the most efficient mechanism for releasing the excess energy is the emission of intense pressure waves. However, in contrast to dry targets—where a bipolar wave profile forms and travels into the bulk[16,26,27]—two distinct compressive waves are here emitted from the interface and propagate into both solid and liquid regions. In a dry target, this stage would be immediately followed by the rapid expansion of the solid. In the wet target, in contrast, the liquid film strongly hampers the expansion of the solid over very long time scales—as long as $t=700\tau^*$; we will return to this important point below.

Given the finite thickness of the liquid film, the pressure wave propagating into the liquid eventually reaches the liquid-vacuum interface (at $t\sim 200\tau^*$ in the present case). Elastic reflection at this interface is not observed (except for very low fluences). Instead, the pressure wave irreversibly affects the topmost layers of the liquid, causing a rapid acceleration and the subsequent formation of a rarefaction wave proceeding toward the solid region, whereby the density decreases significantly. As Figs. 1 and 2 clearly show, the propagation of the rarefaction wave leads to the partial decomposition and ablation of the liquid film through a process which is akin to spallation at the back surface of laser-irradiated films.[28] The expansion of the film causes a gradual weakening of the confinement efficiency of the hot pressurized liquid near the solid-liquid interface, which is then able to expand, leading to the growth of "bubbles" filled with low-density gas, clearly visible in Fig. 1 at $t_4=1500\tau^*$. The bubbles starts to form quite early ($t\sim 200\tau^*$, cf. Fig. 2), but grow very slowly until the rarefaction wave reaches the interface region (around $t=600\tau^*$). The formation of bubbles is thus of thermal origin, but their growth is mediated by the mechanical behavior of the system; thicker films would confine the target more efficiently, but would still allow the growth of bubbles at the interface, albeit at a slower pace. As will be shown below, the presence of bubbles is crucial for significant ablation to take place. As a last point here, we note that the combined effect of the expansion of the liquid near the interface with the solid and the gradual dissipation of the energy stored in the rarefaction wave leaves a large portion of the liquid film relatively intact. The latter is ejected as a whole rather than as clusters, as observed close to the surface of the film; with increasing fluence, the thickness of this liquid layer decreases, more and more of the film being decomposed and ablated as a result of the passage of the rarefaction wave.

The origin of the structural modifications observed in the liquid is best understood in terms of the thermodynamic analysis method introduced in Refs. 14 and 16 (and described in detail therein). The results of this analysis for the simulations presented in Fig. 1 are given in Fig. 3, where we plot the trajectories of various portions ("slices") of the liquid film (as defined by their position z_0 relative to the initial location of the solid-liquid interface) in the density-temperature phase diagram. These trajectories are phase averaged—they are referred to as "average" in Ref. 16—and thus represent the average density and temperature of a slice as a function of time. Evidently, these averages do not provide a complete, detailed picture of the state of the system; for instance, in a two-phase mixture, different states may

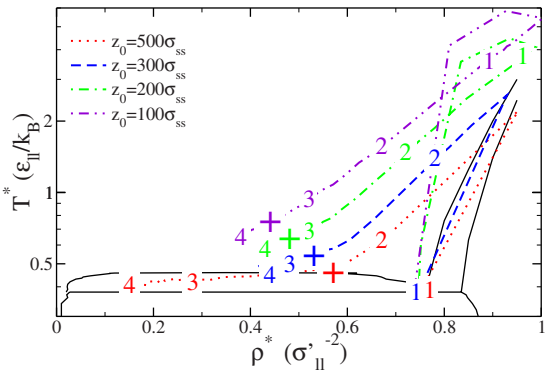

FIG. 3. (Color online) Thermodynamic evolution of the high-density liquid for different values of the position z_0 within the film (measured relative to the initial position of the solid-liquid interface) for a fluence of $560\epsilon_{ss}/\sigma_{ss}$. Red dotted line: $z_0=500\sigma_{ss}$; blue dashed line: $z_0=300\sigma_{ss}$; green dash-dotted line: $z_0=200\sigma_{ss}$; magenta dash-dot-dotted line: $z_0=100\sigma_{ss}$. The numbers ($i=1-4$) refer to the snapshots at t_i in Fig. 1 and the crosses to the moment where density inhomogeneities start to develop (where relevant). The phase diagram (black lines) is described in Ref. 16.

lead to the same average. However, they do demonstrate the effect of confinement. Of course, if a slice is inhomogeneous, a complete thermodynamical characterization requires phase-resolved (i.e., *condensed* and *gas*) trajectories; since these are not essential to the present discussion, they are omitted here for clarity.

Before the arrival of the laser pulse, the liquid is close to the denser end of its triple line and remains there until the pressure wave comes about (recall that the liquid is transparent). The compression of the liquid causes a sudden increase in temperature and pressure, as can clearly be seen by comparing the thermodynamic state of different sections of the film at $t=50\tau^*$ (marked by label 1 on the different z_0 curves): here the wave is at $z\sim250\sigma_{ss}$ and those portions of the film behind it are strongly compressed and heated, while those ahead remain close to the triple point.

The fact that the material does not follow the same thermodynamic path upon compression and decompression (i.e., the material does not return to its initial state upon decompression but rather expands on a higher isentrope) indicates that a significant portion of the energy is dissipated while the pressure wave propagates, leading to the heating of the film. Indeed, decompression occurs at higher temperature than compression, contrary to what is expected for an adiabatic process. Note that heat diffusion from the solid target acts as a further source of heating; this mechanism is of course most important in the interfacial region. As the wave continues to travel, it eventually reaches the liquid-vacuum interface and, as mentioned earlier, is converted into a rarefaction wave, leading to the very rapid decrease of the density of the fluid (cf. labels 2, 3, and 4 on the red dotted line, $z_0=500\sigma_{ss}$). As demonstrated in our previous studies,[14,16] this behavior is typical of a fragmentation process. (Phase explosion is also observed at lower fluences: the material enters the liquid-vapor metastable region in a homogeneous state, following which nucleation and growth of gas bubbles occurs, leading to the disintegration and ablation of the topmost section of the film.) Deeper into the film, expansion also occurs, but at a much slower pace (compare the positions of the labels for the different curves). In this case, the "intact" portion of the film finally settles at a density close to $0.4(\sigma'_{\ell\ell})^{-2}$ (cf. label 4 for $z_0=300\sigma_{ss}$ and $200\sigma_{ss}$); as discussed earlier, this portion of the film is ejected as a whole from the target following the formation of gas bubbles at the solid-liquid interface. Finally, that region of the liquid close to the solid target expands entirely within the supercritical region of the phase diagram (cf. $z_0=100\sigma_{ss}$); the growth of gas bubbles at the solid-liquid interface and the subsequent ejection of the film thus cannot be attributed to phase explosion (which would be subcritical) in this case.

The high- and low-density liquids behave in essentially the same way except that the latter is more readily compressible. This entails two significant consequences: first, because of the reduced speed of sound (by a factor of 9 in the present case), the pressure and rarefaction waves propagate at a lower pace, leading to a slowdown of the dynamics in the liquid film; second, the confinement imposed by the liquid is less efficient in preventing the rapid expansion of the hot and pressurized solid material. In this case, gas bubbles are able to form at the solid-liquid interface even before the rarefaction wave releases the confinement. We will return below to the impact of these differences on the ablation mechanism.

Note that the ejection of an intact liquid layer from a suddenly heated substrate has also been observed in MD simulations of Ar films.[22]

B. Solid target

We now turn to a detailed description of the solid target; we will show that the presence of the liquid film has a very significant impact on the ablation process. In order to establish a proper reference, we begin with a brief discussion of the dry target.

1. Dry solid target

The behavior of dry materials during ultrashort laser ablation has been extensively studied using the present model;[14,16–18] we thus only give a rapid overview of this case here in order to provide a basis for comparison. A typical dry target evolves as displayed in Fig. 4. The first snapshot ($t_1=50\tau^*$) shows that monomers and other very small clusters are ejected first, right after the end of the pulse. During the next $200\tau^*$, the topmost region of the target expands rapidly and disintegrates into a collection of clusters of various sizes, resulting from fragmentation. At the same time, large gas bubbles nucleate and grow deeper into the target, and eventually coalesce, leading to the ejection of a thin liquid layer around $t_4=750\tau^*$; in this case, ablation is attributed to phase explosion.

The thermodynamic evolution of the system is reported in Fig. 5. Close to the surface ($z_0=-50\sigma_{ss}$) the material is found to undergo very rapid heating and subsequent expansion; the latter takes place entirely within the supercritical fluid region (cf. labels 1–4), all the way down to a final, very low-density gaseous state, signaling the occurrence of a vaporization process, as confirmed by the snapshots of Fig. 4. A little further

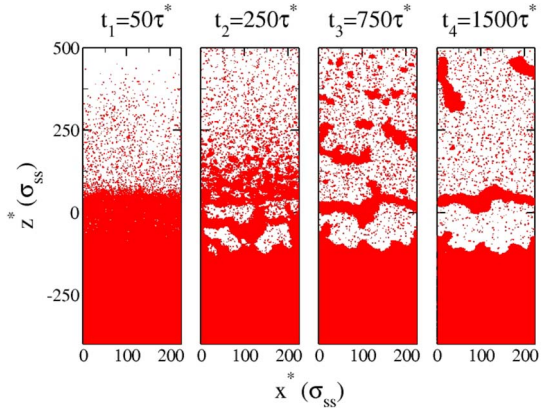

FIG. 4. (Color online) Snapshots of a simulation of a dry solid target at a fluence of $560\epsilon_{ss}/\sigma_{ss}$.

down into the target ($z_0=-100\sigma_{ss}$), fast expansion and gradual disintegration into liquid clusters are observed. As discussed in detail elsewhere,[14,16] the material breaks up during the rapid expansion phase *before* reaching the liquid-vapor coexistence region of the phase diagram; this is the signature of fragmentation. Deeper into the target ($z_0=-150\sigma_{ss}$), the homogeneous liquid enters the liquid-vapor metastable region in a homogeneous state (at 1) and the aforementioned gas bubbles form (between 1 and 4); this is a clear manifestation of phase explosion. Finally, way down into the sample ($z_0=-200\sigma_{ss}$), the energy injected by the laser is insufficient to cause ablation and the material gradually relaxes back to its low-temperature solid state. [We note that the maximum temperature for all trajectories (even subthreshold) may reach very large values; while complex chemical processes may take place at these temperatures in some materials, this does not imply significant ionization as this is usually observed at fluences somewhat higher than those required for supercritical expansion.[7]]

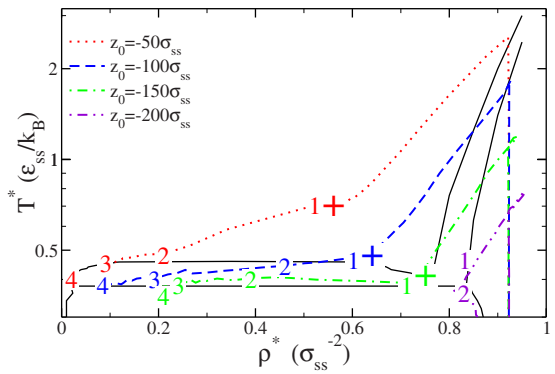

FIG. 5. (Color online) Thermodynamic evolution of a dry solid target for different values of the position z_0 within the target (measured relative to the initial position of the solid-liquid interface) for a fluence of $560\epsilon_{ss}/\sigma_{ss}$. Red dotted line: $z_0=-50\sigma_{ss}$; blue dashed line: $z_0=-100\sigma_{ss}$; green dash-dotted line: $z_0=-150\sigma_{ss}$; magenta dash-dot-dotted line: $z_0=-200\sigma_{ss}$. The numbers ($i=1-4$) refer to the snapshots at t_i in Fig. 4 and the crosses to the moment where density inhomogeneities start to develop (where relevant).

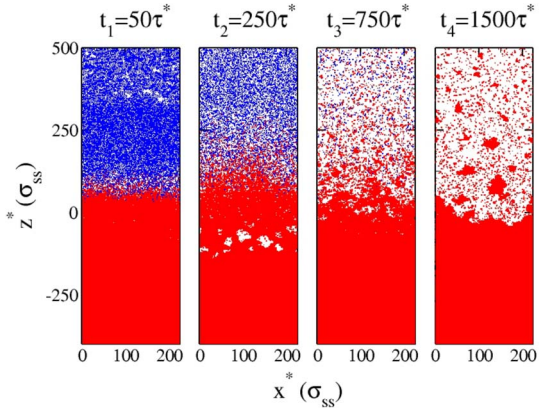

FIG. 6. (Color online) Snapshots of a simulation of a solid target (red dots, bottom) wetted by a low-density liquid (blue dots, top) at a fluence of $560\epsilon_{ss}/\sigma_{ss}$.

2. Solid target wetted by a low-density liquid

We move now to the case of wetting by a low-density liquid, illustrated in Fig. 6. One immediate difference with the dry target (Fig. 4) is the slower expansion rate of the ablated material, roughly by a factor of 5: by $t_1=50\tau^*$, some monomers and small clusters have been ejected from the target (as in the dry case), but they are still confined to a small region near the interface. The evolution of the dry and wetted targets is otherwise similar up to $t_2=250\tau^*$, where both the formation of clusters in the topmost region and the growth of gas bubbles deeper into the sample can be observed. By $t_3=750\tau^*$, however, a very significant difference appears: the gas bubbles within the target have now completely collapsed while cluster formation proceeds. Note that, by this moment, the liquid has been almost completely expelled from the interface region. By $t_4=1500\tau^*$, ablation is complete but the majority of clusters are still close to the target, in contrast to the dry case where only very large clusters remain.

These observations find an echo in the thermodynamic trajectories of Fig. 7: while the behaviors of the two systems are initially similar (compare the locations of points labeled 1 in Figs. 5 and 7), the slowing down of the expansion becomes evident by $t_2=250\tau^*$ (compare label 2); while not sufficient to inhibit completely the formation of clusters close to the interface (dashed line), this causes the gas bubbles deeper down in the target to collapse and hence density to increase (cf. passage from 2 to 3 along the green dot-dashed line). By the end of the simulation, this section of the target is completely outside of the liquid-vapor metastable region (label 4) and actually begins to solidify, relaxing back toward its initial state.

The above results indicate that the effect of the presence of a low-density liquid film is mainly to slow down the expansion of the target. This is sufficient to stop the gas bubbles from growing until coalescence inside the target, hence inhibiting ablation by phase explosion; in contrast, ablation by fragmentation may still occur, and this leads to the ejection of a significant number of clusters. It is worth mentioning that while the dynamics of the system along the dif-

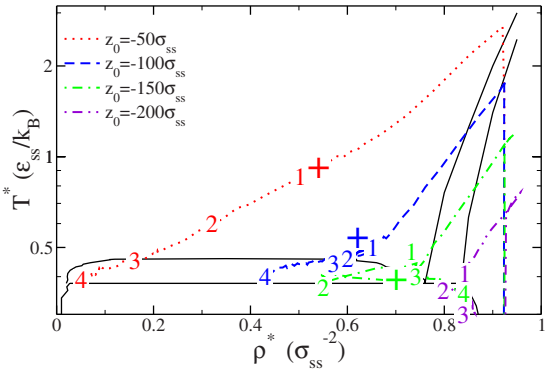

FIG. 7. (Color online) Thermodynamic evolution of a solid target wetted by a low-density liquid for different values of the position z_0 within the target (measured relative to the initial position of the solid-liquid interface) for a fluence of $560\epsilon_{ss}/\sigma_{ss}$. Red dotted line: $z_0=-50\sigma_{ss}$; blue dashed line: $z_0=-100\sigma_{ss}$; green dash-dotted line: $z_0=-150\sigma_{ss}$; magenta dash-dot-dotted line: $z_0=-200\sigma_{ss}$. The numbers ($i=1-4$) refer to the snapshots at t_i in Fig. 6 and the crosses to the moment where density inhomogeneities start to develop (where relevant).

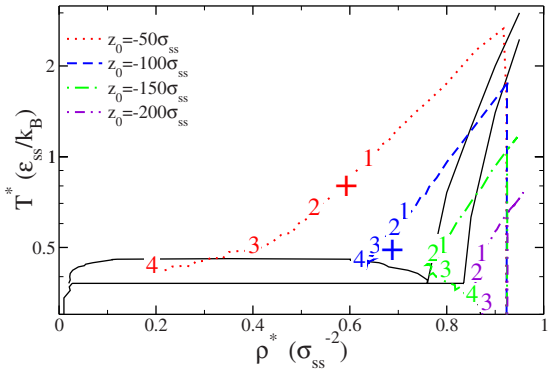

FIG. 9. (Color online) Thermodynamic evolution of a solid target wetted by a high-density liquid for different values of the position z_0 within the target (measured relative to the initial position of the solid-liquid interface) for a fluence of $560\epsilon_{ss}/\sigma_{ss}$. Red dotted line: $z_0=-50\sigma_{ss}$; blue dashed line: $z_0=-100\sigma_{ss}$; green dash-dotted line: $z_0=-150\sigma_{ss}$; magenta dash-dot-dotted line: $z_0=-200\sigma_{ss}$. The numbers ($i=1-4$) refer to the snapshots at t_i in Fig. 8 and the crosses to the moment where density inhomogeneities start to develop (where relevant).

ferent thermodynamic trajectories is strongly affected by the confining effect of the fluid, the general shape of the trajectories themselves is not; this is related to the fact that, given the short time scale over which expansion proceeds, portions of the material having absorbed equivalent amounts of energy will evolve roughly along the same isentropic line.[16]

3. Solid target wetted by a high-density liquid

The behavior observed above is amplified in the case of wetting by a high-density liquid. As can be seen in Fig. 8, the early ejection of monomers now is totally suppressed for $t_3 \leqslant 750\tau^*$, at which point it finally takes place with the concomitant formation of a few clusters; by $t_4=1500\tau^*$, these are finally ejected from the target, following the formation of a low-density layer in the fluid. In this case, the formation of gas bubbles within the target is totally inhibited and only the topmost section of the target undergoes structural modifications.

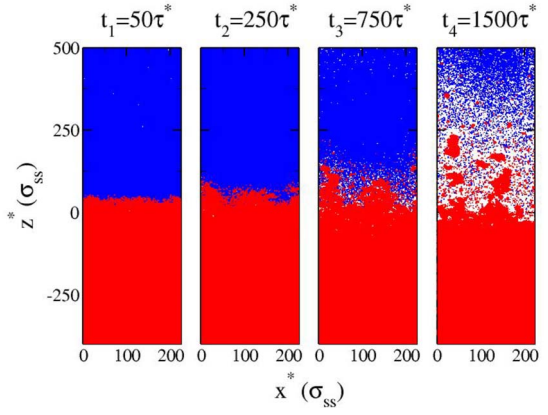

FIG. 8. (Color online) Snapshots of a simulation of a solid target (red dots, bottom) wetted by a high-density liquid (blue dots, top) at a fluence of $560\epsilon_{ss}/\sigma_{ss}$.

The strong confinement of the target by the liquid may also be deduced from the thermodynamic trajectories of Fig. 9. The confinement is now so effective that only the interfacial region (red dotted line) is able to expand significantly. In all other cases, expansion ceases before the liquid-vapor metastable region is reached. This provides further evidence that thermodynamic metastability (and thus phase explosion) is not a necessary ingredient for the formation and ejection of clusters. Finally, the strength of the confinement is also illustrated by the trajectories of portions of the target far from the interface (green dash-dotted line): these do not even melt completely before relaxing back toward the solid state; this contrasts with both the dry and low-density liquid cases, where the trajectory penetrated deep into the metastable region.

4. Properties of the plume

Comparison of the different systems (Figs. 4, 6, and 8) clearly shows that the liquid strongly affects both the ablation process and the properties of the ablated material. We examine the latter aspect in some detail as it is of interest for applications.

As can be seen in Fig. 10, the liquid layer—be it low density or high density—causes a very significant reduction in the ablation yield, and this is particularly evident at low fluence. Thus, the presence of the liquid pushes the ablation threshold to higher fluences; for the high-density liquid, the increase is almost threefold compared to the dry case. The actual form of the dependence of the yield on fluence is also affected by the presence of the liquid: for the dry material, the yield scales logarithmically with fluence,[16] leading to a rapid increase near the threshold and a slower increase at higher fluences; in contrast, for the wet material (particularly in the case of the dense liquid), the yield first increases

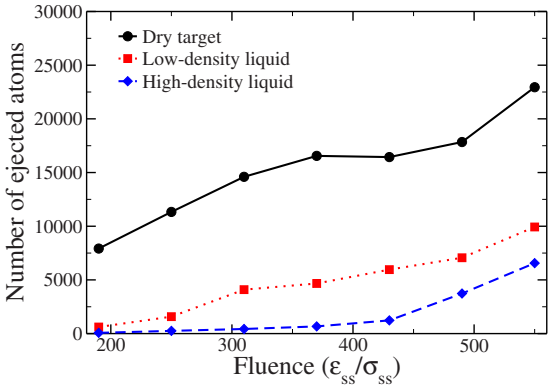

FIG. 10. (Color online) Total number of ejected atoms as a function of fluence. Black continuous line: dry target; red dotted line: target wetted by a low-density liquid; blue dashed line: target wetted by a high-density liquid.

slowly, then more rapidly at higher fluences. Thus, the differences between dry and wet targets become smaller at higher fluences, which is of course expected.

In addition to yield, the structure of the ejected material is also strongly affected by the liquid layer, as can be appreciated from Fig. 11 where the composition of the plume is analyzed. For the dry target, most of the atoms in the plume belong to large clusters (containing more than 1000 atoms) which have been produced through phase explosion. As the fluence increases, fragmentation becomes more important and leads to a larger proportion of atoms within moderate-size clusters (between 11 and 1000 atoms). The proportion of monomers (mainly produced by vaporization) is also seen to increase a bit with fluence; the rest of the plume consists of small clusters (between 2 and 10 atoms). The range of cluster sizes in our simulations is certainly typical of what is observed in experiment.[29,30] For the target wetted by a dense liquid, now, the situation is reversed: at low fluence, the plume contains mostly monomers and small clusters; as the

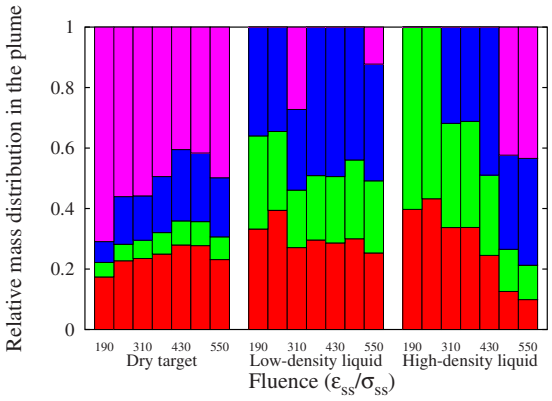

FIG. 11. (Color online) Relative mass distribution in the plume for the dry, low-density, and high-density cases, as a function of fluence. From bottom to top: (red) monomers; (green) atoms in clusters of size between 2 and 10; (blue) atoms in clusters of size between 11 and 1000; (magenta) atoms in clusters larger than 1000 atoms.

fluence increases, these become less popular, with more and more larger clusters being produced by fragmentation. The two effects seem to balance out in the low-density liquid case: the plume mostly consists of momoners and moderate-size clusters, and this is essentially independent of fluence. These differences are mostly due to the complete inhibition of phase explosion in the wet targets, thus suppressing the formation of large clusters in favor of smaller ones produced through fragmentation. The presence of the liquid film thus provides one way of controlling the morphology of the ablations plume, i.e., the distribution in size of the clusters.

Experimental results are in good qualitative agreement with the simulations in spite of significant differences in the thickness of the liquid layer and the range of fluences examined. For instance, femtosecond laser ablation of gold in vacuum and covered by a thin ($\sim$1 mm) water layer reveals the same trend as displayed in Fig. 10 on the ablation threshold and yield.[2,5] Furthermore, the cluster size is found to increase significantly with fluence for the water-covered target,[5] in agreement with the results of Fig. 11. A detailed comparison with the simulation results is, however, difficult as the clusters ejected from the target and penetrating into a relatively thick liquid layer could continue to evolve in size through various chemical reactions (with surfactants or other chemicals present in the liquid) and further aggregation on time scales far larger than can be achieved using atomistic models. In addition, due to the high fluences used in the experiments, the presence of the plasma created into the liquid affects the cluster size distribution possibly through various electronic effects.[5] These complex physical and chemical phenomena are not included in the simulations, and in any case take place over time scales which are much beyond those we are concerned with here. Nevertheless, this comparison suggests that the modifications in the properties of the plume resulting from the presence of the liquid film are not overly sensitive to details of the process as long as confinement is the main factor controlling ablation.

IV. DISCUSSION

Our results indicate that the main consequence of the presence of a liquid film is to confine the hot and pressurized material of the target over long time scales. This is primarily due to inertia: for an incompressible fluid (of which our high-density liquid is a good representation), the expansion of the target (or the formation of large gas bubbles in the film at the interface with the target) requires the displacement of the film as a whole, a process typically occurring on a time scale of $\tau_c = \Delta z_f / c_s$ where c_s is the speed of sound in the liquid and Δz_f is the thickness of the film. Thus, the "quality" of the confinement is expected, in a first approximation, to increase linearly with the thickness of the film. During this period, the target can relax through other channels, such as the diffusion of heat into either the bulk or the film. Furthermore, our results show that the confinement of the target by the film is only gradually lifted, therefore further slowing down its expansion. The combination of these two effects entails a reduced efficiency for the ablation mechanisms which rely on expansion of the target, viz., fragmentation

and, to an even greater extent, phase explosion. However, mechanisms such as vaporization can still occur because they require only local perturbations within the film to take place, consistent with the results presented above.

Of course, real liquids are not incompressible. The effect of the finite compressibility can clearly be seen in the behavior of the low-density liquid film. Indeed, by virtue of the arguments presented above, the quality of the confinement should be higher in this case than for the denser liquid, given the smaller value of the speed of sound in the former. However, our results indicate that it is not so: ablation is more efficient and occurs on a shorter time scale (compare Figs. 6 and 8) with a lighter liquid. This is essentially due to the higher compressibility of the lighter liquid, which enables the rapid formation of a low-density gas region in the film, and thus ablation, even before τ_c is reached. However, even such reduced confinement is sufficient to prohibit the occurrence of phase explosion, in close agreement with the results of Lorazo *et al.*[20] who showed that the occurrence of phase explosion is related to the expansion dynamics of the target. Indeed, low expansion speeds were shown to lead to the collapse of the gas bubbles before the percolation threshold is reached, thus inhibiting ablation. Thus, even a compressible liquid can significantly affect the nature of the ablation mechanisms, and thus the composition of the plume.

The finite compressibility of the liquid also explains why confinement by the film is most effective at low fluence (cf. Fig. 10): the pressure increase inside the target following the absorption of the pulse is modest in this case, and thus easily counteracted by the film. As the fluence increases, so does the pressure in the target, making the compression of the liquid a viable relaxation process, and thus explaining the increase of the ablation efficiency as the fluence increases.

As a final point, it should be mentioned again that our analysis applies only in the thermal regime, i.e., at fluences below the threshold for plasma formation. Above this threshold, the formation and confinement of a plasma at the solid-liquid interface could open alternative routes to ablation. However, comparison of the present results with experiments suggests that the effect of confinement on the plume is qualitatively similar above or below the threshold for plasma formation.

V. CONCLUSION

To summarize, we have studied the ablation by ultrashort laser pulses of solids wetted by liquid films. We find the liquid to play a very significant role in the ablation process, notably by confining the solid over long time scales and slowing down its expansion; this leads to important changes in the dominant ablation mechanisms, principally the suppression of phase explosion. It also causes a strong reduction of the ablation yield and important modifications in the composition of the plume—at fluences above threshold, the size of the ejected nanoclusters is somewhat lower in presence of the liquid; fragmentation and vaporization lead principally to monomers and small clusters, while larger clusters are produced by homogeneous nucleation. Our results provide useful information for achieving better control on the morphology of the clusters generated by pulsed laser ablation.

ACKNOWLEDGMENTS

This work has been supported by grants from the Natural Sciences and Engineering Research Council of Canada and the *Fonds Québécois de la Recherche sur la Nature et les Technologies*. We are grateful to the *Réseau Québécois de Calcul de Haute Performance* for generous allocations of computer resources.

*danny.perez@umontreal.ca
†Author to whom correspondence should be addressed; laurent.lewis@umontreal.ca
‡michel.meunier@polymtl.ca

[1] D. Bauërle, *Laser Processing and Chemistry* (Springer-Verlag, Berlin, 2000).
[2] A. Kabashin and M. Meunier, in *Recent Advances in Laser Processing of Materials*, edited by J. Perrière, E. Milon, and E. Fogarassy (Elsevier, New York, 2006).
[3] G. Yang, Prog. Mater. Sci. **52**, 648 (2007).
[4] A. Kabashin, M. Meunier, C. Kingston, and J. H. T. Luong, J. Phys. Chem. B **107**, 4527 (2003).
[5] A. Kabashin and M. Meunier, J. Appl. Phys. **94**, 7941 (2003).
[6] J.-P. Sylvestre, A. Kabashin, E. Sacher, and M. Meunier, Appl. Phys. A: Mater. Sci. Process. **80**, 753 (2005).
[7] A. Cavalleri, K. Sokolowski-Tinten, J. Bialkowski, M. Schreiner, and D. von der Linde, J. Appl. Phys. **85**, 3301 (1999).
[8] K. Sokolowski-Tinten, J. Bialkowski, A. Cavalleri, D. von der Linde, A. Oparin, J. Meyer-ter-Vehn, and S. I. Anisimov, Phys. Rev. Lett. **81**, 224 (1998).
[9] D. von der Linde and K. Sokolowski-Tinten, Appl. Surf. Sci. **154-155**, 1 (2000).
[10] D. S. Ivanov and L. V. Zhigilei, Phys. Rev. Lett. **91**, 105701 (2003).
[11] V. V. Zhakhovskiĭ, K. Nishihara, S. I. Anisimov, and N. A. Inogamov, JETP Lett. **71**, 167 (2000).
[12] N. M. Bulgakova, R. Stoian, A. Rosenfeld, I. V. Hertel, and E. E. B. Campbell, Phys. Rev. B **69**, 054102 (2004).
[13] L. V. Zhigilei and B. J. Garrison, J. Appl. Phys. **88**, 1281 (2000).
[14] D. Perez and L. J. Lewis, Phys. Rev. Lett. **89**, 255504 (2002).
[15] P. Lorazo, L. J. Lewis, and M. Meunier, Phys. Rev. Lett. **91**, 225502 (2003).
[16] D. Perez and L. J. Lewis, Phys. Rev. B **67**, 184102 (2003).
[17] D. Perez and L. J. Lewis, Appl. Phys. A: Mater. Sci. Process. **79**, 987 (2004).
[18] D. Perez, L. J. Lewis, P. Lorazo, and M. Meunier, Appl. Phys. Lett. **89**, 141907 (2006).
[19] P. Lorazo, D. Perez, L. J. Lewis, and M. Meunier, Proc. SPIE **5448**, 520 (2004).
[20] P. Lorazo, L. J. Lewis, and M. Meunier, Phys. Rev. B **73**, 134108 (2006).
[21] X. Gu and H. M. Urbassek, Appl. Phys. B: Lasers Opt. **81**, 675

(2005).
[22] X. Gu and H. M. Urbassek, Appl. Surf. Sci. **253**, 4142 (2007).
[23] D. Frenkel and B. Smit, *Understanding Molecular Simulations—From Algorithms to Applications* (Academic, San Diego, CA, 1992).
[24] L. V. Zhigilei, E. Leveugle, B. J. Garrison, Y. G. Yingling, and M. I. Zeifman, Chem. Rev. (Washington, D.C.) **103**, 321 (2003).
[25] A. Kruusing, Opt. Lasers Eng. **41**, 329 (2004).
[26] J. C. Bushnell and D. J. McCloskey, J. Appl. Phys. **39**, 5541 (1968).
[27] L. V. Zhigilei, P. B. S. Kodali, and B. J. Garrison, Chem. Phys. Lett. **276**, 269 (1997).
[28] H. Tamura, T. Kohama, K. Kondo, and M. Yoshida, J. Appl. Phys. **89**, 3520 (2001).
[29] S. Amoruso, R. Bruzzese, N. Spinelli, R. Velotta, M. Vitiello, and X. Wang, Europhys. Lett. **67**, 404 (2004).
[30] S. Eliezer, N. Eliaz, E. Grossman, D. Fisher, I. Gouzman, Z. Henis, S. Pecker, Y. Horovitz, M. Fraenkel, S. Maman, and Y. Lereah, Phys. Rev. B **69**, 144119 (2004).